ACS Sustainable Chemistry & Engineering

pubs.acs.org/journal/ascecg

Research Article

Effect of the Lignin Structure on the Physicochemical Properties of Lignin-Grafted-Poly(ε-caprolactone) and Its Application for Water/Oil Separation

Di Xie, Yunqiao Pu, Xianzhi Meng, Nathan D. Bryant, Kailong Zhang, Wei Wang, Arthur J. Ragauskas, and Mi Li*

Cite This: *ACS Sustainable Chem. Eng.* 2022, 10, 16882−16895

Read Online

ACCESS | Metrics & More | Article Recommendations | Supporting Information

ABSTRACT: Lignin-grafted poly(ε-caprolactone) copolymers (lignin-*g*-PCLs) have shown wide application potentials in coatings, biocomposites, and biomedical fields. However, the structural heterogeneity of lignin affecting the structures and properties of lignin-*g*-PCL has been scarcely investigated. Herein, kraft lignin is fractionated into four precursors, namely, F_{ins}, F1, F2, and F3, with declining molecular weights and increased hydroxyl contents. Lignin-*g*-PCLs are synthesized *via* ring-opening polymerization of ε-caprolactone with lignin and characterized by GPC, FTIR, ^{1}H and ^{31}P NMR, DSC, TGA, and iGC. The mechanical properties, UV barrier, and enzymatic biodegradability of the lignin-*g*-PCLs are evaluated. Results show that lignin with a higher molecular weight and aliphatic OH favors the copolymerization, leading to lignin-*g*-PCLs with longer PCL arms. Moreover, lignin incorporation improves the thermal stability, hydrophobicity, and UV-blocking ability but reduces the lipase hydrolyzability of the copolymers. We also demonstrated that the lignin-*g*-PCL-coated filter paper could successfully separate chloroform−, petroleum ether−, and hexane−water mixtures with an efficiency up to 99.2%. The separation efficiency remains above 90% even after 15 cycles. The structural differences of copolymers derived from the fractionation showed minimal influence on the separation efficiency. This work provides new insights into lignin-based copolymerization and the versatility of lignin valorization.

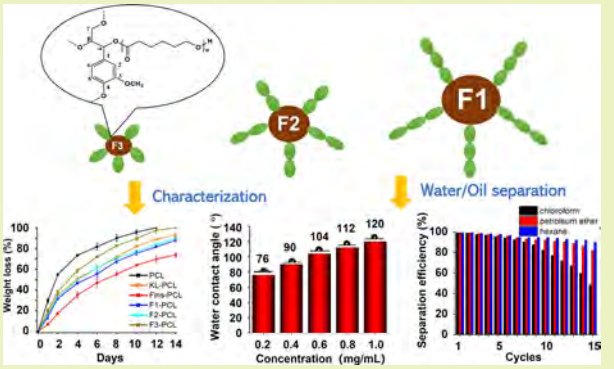

KEYWORDS: *lignin, lignin-g-PCL, structure−property relationship, enzymatic biodegradability, water/oil separation*

INTRODUCTION

Lignin, an abundant, renewable, and biodegradable three-dimensional polymeric macromolecule in plant cell walls, is primarily composed of guaiacyl, syringyl, and hydroxyphenyl subunits.[1] Lignin is typically cataloged as technical lignin (e.g., kraft lignin, alkaline/soda lignin, organosolv lignin) from industrial process and isolated lignin (e.g., milled wood lignin, cellulosic enzymatic lignin, dioxane lignin) depending on the isolation method employed.[2−4] Kraft lignin (KL) produced by the acidification of black liquor from the sulfate pulping process had a worldwide production of approximately 130 million tons in 2015.[5,6] It provides a cheap and readily available source to develop value-added composites, blends, and chemicals[6,7] in addition to the low-value usage for energy generation at pulping mills.[5,8] Furthermore, KL possesses rich phenolic and aliphatic hydroxyls (OHs), providing more versatility for chemical modifications.[9,10] However, the heterogeneous structure of KL, such as molecular weight (MW) and functional groups (amount and types), usually results in nonuniform properties including reactivities, thermal stability, compatibility, solubility, and dispersity. Typically, the aliphatic OH content, glass transition temperature, and thermal stability increase with the augment of lignin MW, while phenolic OH and methoxy contents, solubility, and dispersibility decrease.[11−14] The feedstock heterogeneity could be imparted to the lignin-derived products, leading to disparate performances. For instance, the KL fraction from eucalyptus with a weight-average molecular weight (M_w) of 5,678 Da and a phenolic OH content of 1.42 mmol/g enhanced the ultimate tensile strength of chitosan films; however, the KL fraction with 2,422 Da and 2.17 mmol/g caused an inverse effect.[15] Another study showed that the ethanol-soluble KL fraction from bamboo displayed a benign antimicrobial activity against

Received: September 14, 2022
Revised: November 14, 2022
Published: December 6, 2022

Gram-positive and Gram-negative bacteria growth due to a higher phenolic content and better water solubility as compared to the ethanol-insoluble KL with a lower phenolic content and poor water solubility.[16] Moreover, high-M_w KL fractions from *Pinus caribaea* esterified with succinic anhydride showed better dispersity than their unfractionated counterparts.[17] Therefore, refining KL into more homogeneous feedstock fractions is important to achieve better and desirable product performance.

Poly(ε-caprolactone) (PCL), an aliphatic polyester, shows application potential in plastic replacement, drug delivery, and tissue engineering.[18−20] Due to the biodegradability, good biocompatibility, easy processability, solubility in wide-range solvents, and miscibility with many other polymers, PCL has been widely investigated to copolymerize with lignin *via* ring-opening polymerization (ROP) of ε-caprolactone (ε-CL) to obtain lignin-grafted-PCL copolymers (lignin-*g*-PCLs) that exhibit promising applications in coating,[21] biocomposites,[22] inflammation treatment,[23] and tissue engineering.[24] Our prior work has found that (a) KL can be successfully copolymerized with ε-CL and (b) KL exhibited wider MW distribution than the other technical lignins.[25] Lignin and PCL contribute synergistic impacts to the copolymers. Grafting PCL improves lignin's dispersity, compatibility, and hydrophobicity, and lignin enhances the anti-UV, antioxidation, anti-inflammation, osteo-conductivity, and cell-viability and -proliferation abilities of PCL.[22−26] Lignin-*g*-PCL typifies a star-shaped molecule with a lignin core and PCL arms.[22,27] Technical lignin is reactive to copolymerize with ε-CL irrespective of its botanical sources and extraction methods,[25] but the lignin content negatively affects the MW and thermal properties of the lignin-*g*-PCLs.[28] Moreover, the crystallinity degree (X_c) of the PCL segments in lignin-*g*-PCLs depends on the ε-CL-to-lignin OH (CL/OH) molar ratio to a great extent.[22,27,29] Nevertheless, the reactivities of OHs differ among different OH types in terms of phenolic, aliphatic, and carboxylic OHs,[30,31] so simply applying CL/OH as a variant is insufficient to reveal the synthetic mechanism.

Different structural characteristics of lignin-*g*-PCLs lead to different physicochemical properties. The thermal properties of lignin-*g*-PCLs depend on the length of grafted PCL chains.[29] The lignin-*g*-PCLs become brittle when the PCL portion is semi-crystalline due to the phase separation between PCL and lignin, while they become flexible when the PCL portion is amorphous due to the interval of molar mass among PCL chains.[27] Besides, the elongation at the break of lignin-*g*-PCLs is linked with both the PCL chain length and the number of grafted PCL chains.[27] In addition, an elastomeric behavior can be observed when the length of PCL chains is in a certain range (between 7 and 11).[27] Nevertheless, the effect of the lignin structure, including MW and OH content, on the structures and properties of lignin-*g*-PCL has not been studied. According to the Hansen solubility parameter, boiling point, and heat of vaporization, sequential-solvent fractionation using the binary methanol−acetone solvent system and aprotic hexane as the antisolvent is an easy and effective approach to achieve structurally customized fractions of lignin (e.g., narrow-ranged MWs and varied OHs).[14] We postulated that using lignin fractions with more controlled structural features as the feedstock for copolymerization will lead to distinguished features and properties of lignin-derived products, which will facilitate the valorization of lignin.[32]

In this work, structurally heterogeneous KL was first fractionated using a binary solvent and antisolvent sequential approach into different fractions with representative MWs and OH features. The lignin fractions were subsequently copolymerized with ε-CL to obtain lignin-*g*-PCLs *via* ROP. The structure and physicochemical properties of the synthesized lignin-*g*-PCLs were investigated to establish a "structure−property" relationship. The biodegradability of lignin-*g*-PCLs was also measured by lipase hydrolysis. Inspired by the naturally water-resistance function, lignin has been widely applied to fabricate hydrophobic filtration or absorption materials for water/oil separation.[33−36] We used lignin-*g*-PCLs to coat on filter paper (FP) for separating water and oil mixtures to explore new applications of lignin-*g*-PCLs. The present study is expected to provide a fundamental understanding of lignin copolymerization and advance lignin biorefinery and valorization.

EXPERIMENTAL SECTION

Materials. Southern pine softwood KL, isolated *via* the LignoBoost process, was provided by Domtar Co. (SC, USA). PCL (M_w ∼ 14,000 Da), ε-CL, stannous octanoate ($SnOct_2$), acetone, hexane, methanol, ethanol, chloroform ($CHCl_3$), acetic anhydride, tetrahydrofuran (THF), 2-chloro-4,4,5,5-tetramethyl-1,3,2-dioxaphospholane (TMDP, 95%), deuterated chloroform ($CDCl_3$, 99.8%), *N*-hydroxy-5-norbene-2,3-dicarboxylic acid imide (NHND), nonane, octane, heptane, acetonitrile, ethyl acetate, dichloromethane, petroleum ether, lipase (from *Pseudomonas fluorescens*), silicon dioxide (SiO_2), and silicone oil were purchased from Sigma Aldrich (St. Louis, MO). Anhydrous pyridine was purchased from Spectrum Chemical (New Brunswick, NJ). All chemicals were used as received.

Lignin Fractionation. KL was fractioned into four different fractions with different MWs according to the previous report[14] with some modifications (Figure S1). Briefly, 10 g of KL was dissolved in 50 mL of acetone−methanol cosolvent (7:3, *v*/*v*), and the suspension was centrifuged (10,000 rpm, 10 min, 4 °C) to obtain and separate the insoluble fraction (F_{ins}) and supernatant. Next, 5 mL of hexane antisolvent was added to the supernatant, followed by centrifugation to isolate the precipitate (F1) and the supernatant. The addition of hexane was repeated to collect another precipitate (F2), and the soluble part was concentrated into a solid (F3) by rotary evaporation. The yields of F_{ins}, F1, F2, and F3 are 2.45, 1.47, 4.72, and 73.31%, respectively. The four lignin fractions were further dried in a vacuum oven.

Synthesis of Lignin-*g*-PCLs. KL and the four lignin fractions were, respectively, copolymerized by the solvent-free ROP of ε-CL monomers.[25] In brief, vacuum-dried lignin samples, ε-CL (CL/OH molar ratio of 10, the lignin OH content was measured by ^{31}P NMR), and 0.2 wt % catalyst $SnOct_2$ (based on the ε-CL amount) were reacted under stirring at 130 °C and a N_2 atmosphere for 24 h. The crude product was then recovered by adding cold methanol dropwise. Subsequently, it was thoroughly washed with cold methanol to remove ε-CL monomers and neat PCL. The product was air-dried for 24 h, followed by vacuum drying at 25 °C for 12 h to obtain lignin-*g*-PCL copolymers, which were named KL-PCL, F_{ins}-PCL, F1-PCL, F2-PCL, and F3-PCL corresponding to the feedstocks KL, F_{ins}, F1, F2, and F3, respectively.

Characterization of Lignin-*g*-PCLs and Lignin-*g*-PCL Films. Gel permeation chromatographic (GPC) was applied to determine the M_w and number-average molecular weight (M_n) of acetylated lignin and lignin-*g*-PCL copolymers. The molar-mass dispersity ($Đ_M$) is defined as the ratio of M_w to M_n. The acetylation was carried out in pyridine/acetic anhydride (1:1, v/v) based on previous work.[25] The acetylated lignin and lignin-*g*-PCL copolymers were dissolved in THF and then filtered through a nylon filter with a pore size of 0.45 μm for GPC analysis. Size-exclusion separation was performed on an Agilent 1200 HPLC system (Agilent Technologies, Inc., Santa Clara, CA, USA) equipped with Waters Styragel columns (HR1, HR2, and HR6;

https://doi.org/10.1021/acssuschemeng.2c05495
ACS Sustainable Chem. Eng. 2022, 10, 16882−16895

Table 1. Weight-Average (M_w), Number-Average (M_n) Molecular Weight, and Molar-Mass Dispersity ($Đ_M$) of Lignin and Lignin-*g*-PCLs Measured by GPC and the Average Length of PCL Arms Measured by ^{1}H NMR

	M_w (Da)	M_n (Da)	$Đ_M$		M_w (Da)	M_n (Da)	$Đ_M$	PCL size
	Lignin and Lignin Fractions				Lignin-*g*-PCLs			
KL	3,801 ± 16	1,072 ± 194	3.55 ± 0.64	KL-PCL	44,775 ± 1100	19,789 ± 1084	2.21 ± 0.07	32
F_{ins}	11,188 ± 1011	1,983 ± 39	5.64 ± 1.21	F_{ins}-PCL	13,472 ± 190	4,268 ± 186	3.16 ± 0.18	7
F1	4,461 ± 233	1,556 ± 12	2.87 ± 0.89	F1-PCL	57,143 ± 1466	29,262 ± 120	1.95 ± 0.04	40
F2	3,086 ± 295	1,090 ± 53	2.83 ± 0.46	F2-PCL	38,834 ± 181	17,240 ± 96	2.25 ± 0.00	25
F3	1,691 ± 100	779 ± 44	2.17 ± 0.31	F3-PCL	28,686 ± 248	12,432 ± 122	2.31 ± 0.04	20

Waters Corporation, Milford, MA, USA) and an ultraviolet detector (wavelength: 270 nm). THF was used as the mobile phase at a flow rate of 0.5 mL/min, and polystyrene was used as a standard for calibration. The values were calculated by the averages of the duplicate sample with standard deviations.

Fourier transform infrared (FTIR) spectroscopic analyses of samples were performed using an FTIR spectrometer (Spectrum One FTIR system, PerkinElmer, Wellesley, MA) with a universal attenuated total reflection accessory. Wavenumbers ranged from 4,000 to 600 cm^{-1} for 32 scans with a resolution of 4 cm^{-1}. Nuclear magnetic resonance (NMR) spectral data were recorded using a Bruker Avance III HD 500 MHz spectrometer. 50 mg of lignin-*g*-PCL copolymers was dissolved in 0.5 mL of $CDCl_3$ and then transferred to a 5 mL NMR tube for ^{1}H NMR. ^{1}H NMR was used on a BBO probe with a spectra width 10 ppm, 16 transients, and a 2 s pulse delay by employing a 1D-sequence "zg30" with a 30° flip angle at room temperature. The central $CDCl_3$ solvent peak at a chemical shift (δ) of 7.26 ppm was used for chemical shift calibration. ^{1}H NMR was used to characterize the structure of lignin-*g*-PCL and calculate the average length of PCL arms (PCL size) grafted to lignin by the integration ratio of repeating $-CH_2O-$ units to $-CH_2OH-$ end group of the PCL segment.[22] An inverse-gated decoupling pulse sequence (Waltz-16) was used for quantitative ^{31}P NMR experiments. The OHs were quantified according to the literature based on an internal standard of NHND.[37] The acquired spectra were processed using Bruker Topspin 3.5 software. Assignments of compositional subunits were referred to the reported literatures.[22,25]

Differential scanning calorimetric (DSC) and thermal gravimetric analysis (TGA) were carried out using a Q-2000 differential scanning calorimeter (TA Instruments, USA) and a Q-50 thermogravimetric analyzer (TA Instruments, USA), respectively. For the DSC measurement, about 5 mg of each sample was hermetically sealed in an aluminum pan and then subjected to a heating and cooling cycle twice, from 30 to 100 °C, at a rate of 10 °C/min under a nitrogen atmosphere. The second scanning DSC heating and cooling curves were used to determine the melting (T_m) and crystallization (T_c) temperatures and X_c.[25] For the TGA measurement, around 5 mg of each sample was loaded into the ceramic crucible for heating from 30 to 800 °C at a rate of 10 °C/min under N_2. The onset temperature of thermal degradation (T_{onset}) and the temperature at the maximum mass loss (T_{max}) are determined by TGA and differential TGA (DTG) curves. Universal Analysis 2000 software was applied to analyze the data.

Inverse gas chromatography (iGC) experiments were conducted using an IGC surface energy analyzer (SEA) equipped with a flame ionization detector (Surface Measurements Systems (SMS), Ltd., Alperton, UK). Approximately 80 mg of the dried sample was packed into an individual silanized glass column (length: 300 mm, inner diameter: 4 mm) using the SMS column packing accessory. Samples were injected by *n*-alkanes (nonane, octane, heptane, and hexane) and polar probe molecules (acetone, ethanol, acetonitrile, ethyl acetate, and dichloromethane) to determine the dispersive (γ_d) and specific (γ_{sp}) surface energies over surface coverage between 0.01 and 0.4 n/nm. Data were analyzed by advanced SEA analysis software (Advance Version 1.4.2.0).

PCL and lignin-*g*-PCL copolymer films were prepared using hot compression[22] under 0.1 MPa pressure at 60 °C to obtain films with a thickness of 2 mm. The films were cooled down in an ambient environment before measuring mechanical, UV-blocking, and biodegradable properties. Mechanical properties were measured using an Instron 5943 universal tensile tester (Instron Co., USA) according to the standard ASTM 882-10.[38] With some modifications from previous literature,[39] the coupons were prepared and cut from the prepared films as a rectangle shape with 5 cm length and 1 cm width for mechanical property measurements. Each rectangular coupon was stretched with an initial grip separation and a crosshead speed of 50 mm/min at room temperature. The average values of five replicates are reported for each film.

The UV-protection ability of films was evaluated according to a literature method[40] using UV−vis spectra as a function of light wavelength (ranges from 200 to 800 nm) against transmission recorded by an Evolution 60S UV−vis spectrometer (Thermo Fisher Scientific, USA).

Enzymatic Biodegradation of Lignin-*g*-PCL Films. Enzymatic hydrolysis was used to assess the biodegradability of neat PCL and lignin-*g*-PCLs using a modified method.[41] In brief, lipase solution was prepared by dissolving amino lipase from *Pseudomonas fluorescens* in phosphate-buffered solution (pH = 8) to a concentration of 400 U/mL. Each specimen (10 × 10 × 0.2 mm^3) in triplicates was weighed, added to a 5 mL enzymatic solution, and placed in a shaker at 250 rpm under 45 °C. Specimens were taken out, washed twice with DI water, air-dried, weighed, and returned to the vials with a 5 mL fresh lipase solution every 2 days for 2 weeks. The biodegradability was calculated by the weight loss of samples as a function of time.

Water/Oil Separation with Lignin-*g*-PCLs-Coated Filter Paper. Coated filter paper (CFP) was prepared based on published method[33] with minor modifications. FP was soaked in different concentrations (0.2, 0.4, 0.6, 0.8, and 1.0 mg/mL) of F1-PCL/acetone solutions for 12 h, followed by solvent evaporation. Next, SiO_2 was dispersed well in silicone oil for the second impregnation for 2 h and then stabilized under 40 °C for 6 h for further characterization. Neat PCL in acetone at a concentration of 1.0 mg/mL was coated with the same procedure as a comparison. CFP-Blank (CFP-B) was prepared by coating only the SiO_2/silicone oil mixture. FPs were coated with different copolymers (i.e., KL-PCL, F_{ins}-PCL, F1-PCL, F2-PCL, and F3-PCL) under the same concentration of 1 mg/mL to select the best one for further comparisons. FP coated with PCL and selected F1-PCL at a concentration of 1.0 mg/mL in acetone are named CFP-P and CFP-C, respectively. The water contact angle (WCA) and surface morphology of CFPs were measured using a contact angle goniometer (Ramé-Hart Instrument Co., USA) and a scanning electron microscope (Zeiss Auriga, Germany), respectively.

Water/oil separation tests were conducted using a simple and convenient conical funnel setup with coated FP to separate water (dyed purple) from organic solvents (dyed orange), including petroleum ether, hexane, and chloroform.[42] The organic solvent/water mixtures were prepared by mixing 5 mL of organic solvent and 5 mL of water. The mixed liquid was added to the funnel, and the separation ended when no droplet fell. The filtration efficiency (%) was calculated by the weight percentage of stopped water in the funnel over originally added water in mixed liquid at room temperature. To evaluate the reusability of CFP-C, the filtration efficiencies of continuously used CFP-C during 15 cycles were recorded.

https://doi.org/10.1021/acssuschemeng.2c05495
ACS Sustainable Chem. Eng. 2022, 10, 16882−16895

RESULTS AND DISCUSSION

Lignin Fractionation. The successive fractionation of KL (M_w = 3,801 ± 16 Da) using the cosolvent of acetone−methanol (7:3, *v*/*v*) and antisolvent of hexane resulted in four fractions with different M_w from high to low, namely, F_{ins} (11,188 ± 1011 Da), F1 (4,461 ± 233 Da), F2 (3,086 ± 295 Da), and F3 (1,691 ± 100 Da) (Table 1). KL was well dissolved in acetone−methanol cosolvent due to their high hydrogen bonding capacities and the plasticizing effect of methanol owing to its small molecular size, which promotes the diffusion of organic cosolvent molecules into the compact lignin complexes.[14] When hexane was added, the difference between the Hansen solubility parameters of solvent and lignin increased remarkably, resulting in the precipitation of large lignin molecules. In contrast, lignin oligomers (low-M_w lignin) remain soluble in the solvents because of their wider range of hydrogen bonding ability and Hansen solubility parameter than high-M_w counterparts until an extra amount of antisolvent is added.[43] Consequently, lignin fractions with declining M_w were sequentially precipitated upon the amount of hexane addition in this work. Compared with the successive precipitation method using acetone followed by methanol,[44] F_{ins} in this work precipitated from the lignin dissolved by the acetone−methanol cosolvent had a higher M_w (11,188 *vs* 9,430 Da), suggesting that the acetone−methanol cosolvent can dissolve more high-M_w lignin than a single solvent. The F_{ins} had a wider $Đ_M$ than KL, which may be due to the presence of carbohydrates and/or lignin−carbohydrate complex of which the M_w is much different from that of lignin.[14,45] On the contrary, the $Đ_M$ of the other three fractions, F1, F2, and F3, are in the range from 2 to 3 smaller than that of KL (Table 1) and are comparable with the previously reported $Đ_M$ of 1.4−2.2[21] and 1.5−2.5,[45] suggesting that the acetone−methanol cosolvent fractionation method used in this work effectively refines KL into more uniform fractions.

As the OH groups of lignin are important structural elements that serve as the initial sites for the ROP of ε-CL,[29] we have quantified the OHs of the four lignin fractions using ^{31}P NMR spectroscopy. The aliphatic, phenolic (including C_5-substituted, guaiacyl, and *p*-hydroxyphenyl OHs), and carboxylic OHs were identified and well-resolved in the ^{31}P NMR spectra (Figure 1).[37] The quantitative contents of the total, phenolic, aliphatic, and carboxylic OHs are 5.95 ± 0.03, 3.56 ± 0.02, 1.89 ± 0.01, and 0.50 ± 0.00 mmol/g in KL (Table 2), respectively, which are comparable with those reported studies on industrial softwood KLs.[14,25] The high phenolic OH content is attributed to the cleavage of alkyl aryl ether bonds (such as β-O-4 and α-O-4) during the pulping process, releasing more phenolic OH at the lignin aromatic rings.[11,44]

Previous studies have shown that the lignin aliphatic OH content increases, while the phenolic OH content decreases along with the increase of lignin M_w.[11,14,45] The correlation and regression analyses of the three representative lignin fractions (i.e., F1, F2, and F3) in the current study are consistent with this relationship. In other words, lignin M_w has a positively linear correlation with the quantity of aliphatic OH [Pearson correlation coefficient (r) = 1.000, regression coefficient (R^2) = 1.00, *P* value (P) = 0.189] and a negatively linear correlation with the quantity of phenolic OH (r = −0.999, R^2 = 1.00, P = 0.031) (Figure 2A). The phenolic OH concentration increases with the reduction of lignin M_w, which may be due to the following factors: (1) β-*O*-4 linkages are cleaved with the addition of hexane, forming new phenolic OHs,[14,46] (2) phenolic OH itself is the chain end of the lignin oligomers,[30] which means that the low-M_w lignin fraction has a high frequency of phenolic OH.[47] The elevation of the phenolic OH content leads to a decreased proportion of aliphatic OHs. Also, it helps to explain why the phenolic OH concentration is much lower in F_{ins} than in other lignin fractions (Table 2).

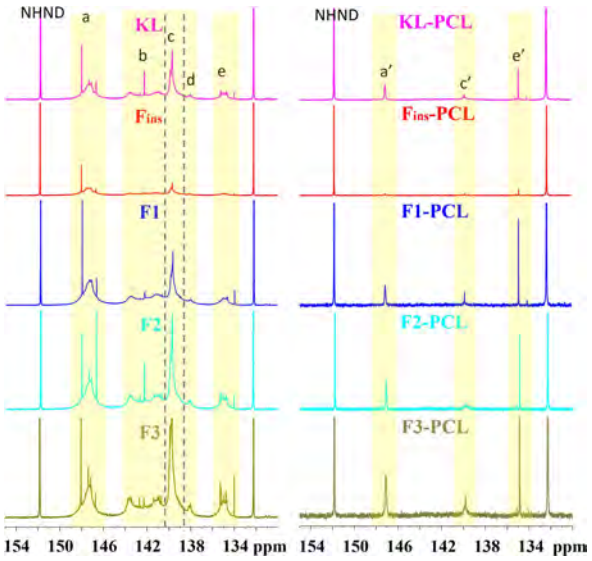

Figure 1. ^{31}P NMR spectra of lignin fractions (left) and lignin-*g*-PCLs (right). (a) aliphatic OH, (b) C_5-substituted OH, (c) guaiacyl OH, (d) *p*-hydroxyphenyl OH, and (e) carboxylic OH.

In sum, the obtained F1, F2, and F3 fractions are representative lignin fractions featuring declining M_w and aliphatic OH content but increased phenolic OH content. However, F_{ins} is not counted as a representative lignin fraction in this study because of its unusually high M_w, wide $Đ_M$, and low OH content, which will presumably hinder its ROP due to poor solubility and dispersibility, unfavorable homogeneity, and limited reactive sites. Besides, the poor solubility of F_{ins} in $CDCl_3$ led to an underestimated quantitation of the OH content by ^{31}P NMR.

Structural Characterization of Lignin-*g*-PCLs. ^{31}P NMR spectra confirmed the successful grafting copolymerization of lignin and PCL due to the substantially diminished phosphitylated OH peaks for the copolymers in comparison to the lignin feedstock in the current work. The ROP of ε-CL with aliphatic and phenolic OHs of lignin leads to the PCL segment ending with aliphatic OH at 145.4−150 ppm (a′ in Figure 1); ε-CL reacting with carboxylic OHs leads to carboxylic OH at the end of the PCL segment shown by the peak at 133.6−136.0 ppm (e′ in Figure 1). ROP of ε-CL itself can afford a PCL linear homopolymer bearing both aliphatic OH and carboxylic OH in equivalent quantity. First, lignin-*g*-PCLs exhibit fewer OH signals (a′, c′, and e′) than their corresponding lignin fractions (a, b, c, d, and e) (Figure 1). The disappearance of both signal b assigned to C_5-substituted OH at 144.5−140.0 ppm and d assigned to *p*-hydroxyphenyl OH at 137.0−139.0 ppm after synthesis indicates that they were replaced by PCL arms ended with aliphatic OHs. Second, compared with corresponding lignin fractions, the decreased aliphatic OH concentration in lignin-*g*-PCLs (Table 2) implies successful ROP occurrence because introducing PCL arms

https://doi.org/10.1021/acssuschemeng.2c05495
ACS Sustainable Chem. Eng. 2022, 10, 16882−16895

Table 2. Quantification of Hydroxyl Groups in Lignin and Lignin-*g*-PCLs by ^{31}P NMR

OH types (mmol/g)	aliphatic	C_5 substituted	guaiacyl	*p*-hydroxyphenyl	carboxylic	total phenolic	total
			Lignin				
KL	1.89 ± 0.01	1.54 ± 0.17	1.85 ± 0.17	0.17 ± 0.03	0.50 ± 0.00	3.56 ± 0.02	5.95 ± 0.03
F_{ins}	0.66 ± 0.00	0.27 ± 0.01	0.36 ± 0.02	0.01 ± 0.00	0.01 ± 0.00	0.63 ± 0.01	1.30 ± 0.01
F1	2.15 ± 0.04	1.80 ± 0.05	1.38 ± 0.03	0.15 ± 0.01	0.45 ± 0.01	3.33 ± 0.01	5.92 ± 0.02
F2	1.82 ± 0.01	1.72 ± 0.02	1.72 ± 0.02	0.22 ± 0.02	0.48 ± 0.01	3.73 ± 0.00	6.03 ± 0.03
F3	1.52 ± 0.05	1.81 ± 0.04	1.81 ± 0.04	0.20 ± 0.00	0.58 ± 0.01	4.21 ± 0.04	6.31 ± 0.02
			Lignin-*g*-PCLs				
KL-PCL	0.33 ± 0.01	UD[a]	0.25 ± 0.01	UD	0.21 ± 0.01	0.25 ± 0.01	0.79 ± 0.00
F_{ins}-PCL	0.18 ± 0.01	UD	0.11 ± 0.00	UD	0.16 ± 0.01	0.12 ± 0.00	0.45 ± 0.01
F1-PCL	0.46 ± 0.01	UD	0.21 ± 0.00	UD	0.33 ± 0.01	0.21 ± 0.00	1.00 ± 0.00
F2-PCL	0.66 ± 0.01	UD	0.33 ± 0.00	UD	0.40 ± 0.01	0.33 ± 0.01	1.39 ± 0.00
F3-PCL	0.77 ± 0.01	UD	0.46 ± 0.01	UD	0.57 ± 0.02	0.45 ± 0.01	1.80 ± 0.00

[a]UD: undetected.

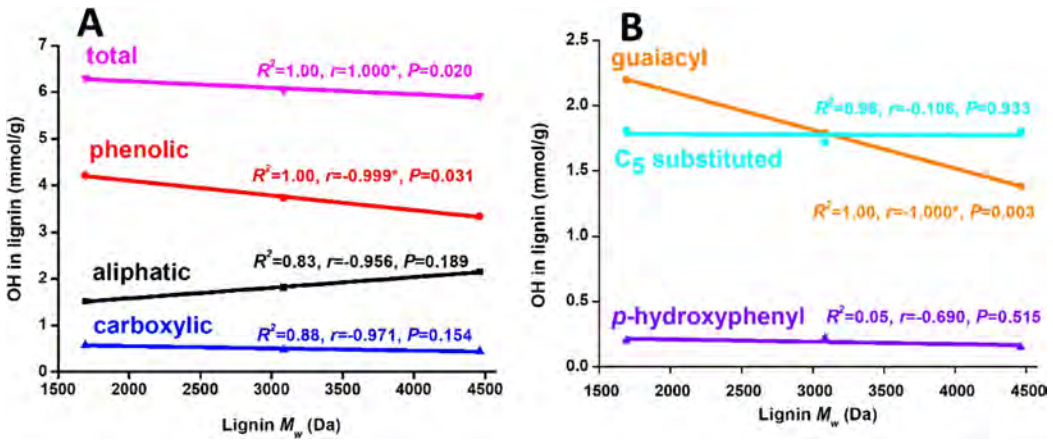

Figure 2. Relation of lignin M_w with the OH content (A) and phenolic OH content (B). *r*: Pearson correlation coefficient; *P*: *P* value; R^2: regression coefficient; *: statistical significance.

increases the product mass and thus reduces the concentration of aliphatic OH as the absolute total OH quantity is constant. Thirdly, the barely diminished carboxylic OH content (Table 2) might be attributed to the end carboxylic OH introduced by PCL chains. Lastly, neat PCL possesses one aliphatic OH and one carboxylic OH located at each chain end.[25] If PCL was physically mixed with lignin OH, combined with M_w results where the lignin portion is negligible compared with massive PCL portion, the products would still show a nearly equivalent quantity of aliphatic and carboxylic OH. However, the amount of terminal aliphatic OH is higher than that of end carboxylic OH in lignin-*g*-PCLs (Table 2), validating the formation of covalent linkages between lignin and PCL.

The reactivity of OHs with *ε*-CL varies on the chemistry of OHs, for example, aliphatic, phenolic, and carboxylic OHs. In this study, the OH decreasing percentage is defined as the ratio of the declined OH content after copolymerization to the original OH content in lignin, revealing the reaction degree of the OH. From the plots exhibiting the OH decreasing percentage of different types of OHs against the three fractions (Figure 3C), the magnitudes of decreasing percentages of all OH types increase as lignin M_w increases (Figure 3C), suggesting easier copolymerization between higher-M_w lignin and *ε*-CL. The aliphatic OH is positively correlated with the copolymer M_w with statistical significance (r = 0.997, R^2 = 0.99, and P = 0.045, Figure 3D), implying that the aliphatic OH is the most reactive grafting site for PCL segments despite the introduction of a new aliphatic OH end to the copolymers. Our group has previously shown that the copolymerization reaction tends to occur preferentially at the aliphatic OHs rather than at the phenolic OHs of lignin.[25] Another study by Najarro et al. showed a similar discovery that the PCL oligomers were mainly introduced to the aliphatic OHs in lignin, leaving the phenolic OH unmodified at a low CL/OH molar ratio (i.e., 5/1) and completely reacted at a high ratio (i.e., 25/1).[48] This was explained by the resistance of phenolic OHs that were not activated to form the alkoxide, and in consequence, there was no activation of the OH or acyl C−O bonds with the monomer. We think this phenomenon can also be explained by the higher nucleophilicity (stronger reactivity) and less steric hindrance effect of the aliphatic OHs toward *ε*-CL than phenolic OHs.[30,49]

The MW of the synthesized lignin-*g*-PCLs provides critical information to indicate (*i*) the reactivity of lignin fractions and (*ii*) the structure of obtained copolymers. With respect to the M_w of synthetic copolymers, F_{ins}-PCL increases slightly from 11,188 to 13,472 Da, and the average length of PCL arms grafted to the lignin is only 7 (Table 1). The limited degree of grafting copolymerization of F_{ins}-PCL is attributed to the limited number of OH-grafting sites in F_{ins} (Table 2), as well as the poor solubility and dispersity of F_{ins} in *ε*-CL due to its high M_w and "xylan impurities" detected by the ^{1}H NMR spectrum of F_{ins}-PCL at 4.32 ppm[50] (Figure S2). Besides, the M_w of the other three copolymers is significantly higher than that of their corresponding lignin fractions (Table 1), indicating that the M_w of copolymers is predominated by the PCL segment

https://doi.org/10.1021/acssuschemeng.2c05495
ACS Sustainable Chem. Eng. 2022, 10, 16882−16895

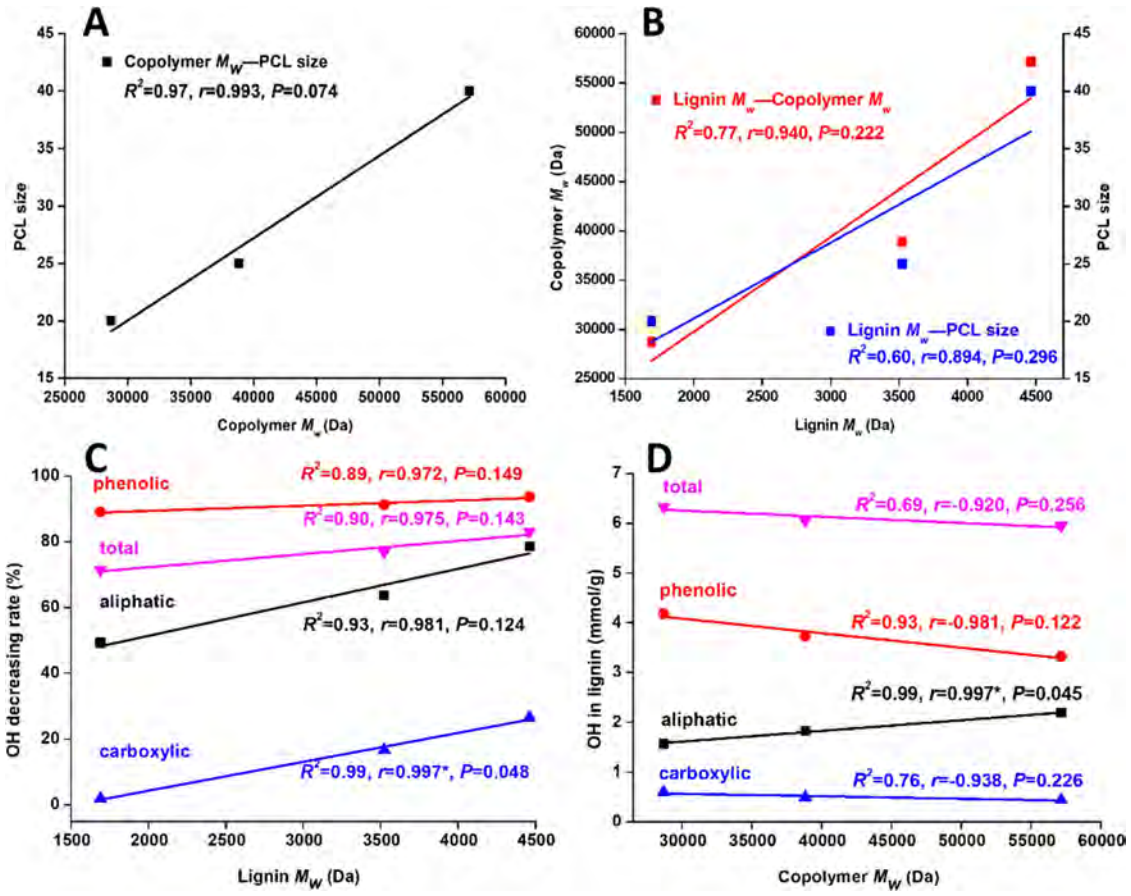

Figure 3. Relations of copolymer M_w with the PCL size (A), lignin M_w with copolymer M_w and PCL size (B), lignin M_w with the OH decreasing percentage (C), and copolymer M_w with the OH content in their corresponding lignin fraction (D). r: Pearson correlation coefficient; P: P value; R^2: regression coefficient; *: statistical significance.

instead of the lignin core. The conclusion is also revealed by the positive correlation between copolymer M_w and the PCL size (r = 0.993, R^2 = 0.97, Figure 3A). In addition, both copolymer M_w and the PCL size reveal a positive relationship with lignin M_w (r > 0.85, Figure 3B), implying that high-M_w lignin is beneficial to the formation of long-chain PCL arms and high-M_w lignin-*g*-PCLs. The reason might be that high-M_w lignin has more aliphatic OH with stronger reactivity with ε-CL. Overall, copolymer M_w highly depends on the aliphatic OH concentration that is positively related to the M_w of lignin fractions.

The FTIR spectra confirmed that lignin-*g*-PCLs are featured with the characteristic absorbance of both lignin and PCL, evidencing successful ROP of ε-CL grafted to lignin (Figure 4). The peaks at 1,596 and 1,513 cm^{-1} are attributed to the aromatic skeleton vibration of lignin,[51] indicating the presence of the lignin constituent in the produced copolymers. The O−H stretching absorption bands located at 3,382 and 3,432 cm^{-1} are found in the spectra of KL and copolymers, respectively, showing a blue shift in wavenumber after copolymerization, which might be attributed to the intermolecular hydrogen bonding.[25,29] The weaker band intensity of OH in copolymers than in KL spectra endorses the results that the OH content reduces after the ROP reaction, meaning that the lignin is covalently linked with the PCL segment rather than physical blending, which agrees with our ^{31}P NMR results. Thirdly, the remarkably stronger C−H stretching (2,950−2,830 cm^{-1}) and bending signals (1,460−1,360 cm^{-1} and 731 cm^{-1}) of methyl

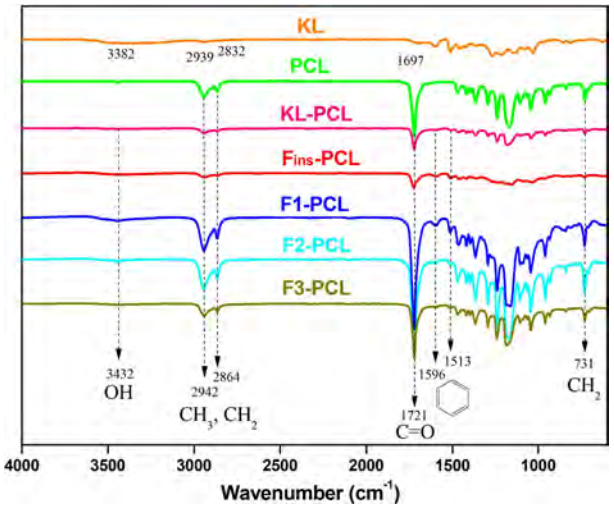

Figure 4. FTIR-ATR spectra of KL, PCL, and lignin-*g*-PCLs.

(CH_3) and methylene (CH_2) groups in copolymers than those in the KL spectrum are also detected, implying the presence of the PCL constituent in the produced copolymers.[29] Lastly, the weak peak at 1,697 cm^{-1} and intensified peak at 1,721 cm^{-1} correspond to carbonyl groups in KL and copolymers, respectively,[25] and the signal strengthening and shift in copolymers could be explained by the formation of strong intermolecular hydrogen bonds with lignin OHs.[28,29,52]

https://doi.org/10.1021/acssuschemeng.2c05495
ACS Sustainable Chem. Eng. 2022, 10, 16882−16895

Physicochemical Properties of Lignin-*g*-PCLs. The crystalline degree and thermal properties of the lignin-*g*-PCLs derived from different lignin fractions were determined and compared using DSC and TGA. Generally, the neat PCL has an X_c of 73.3%, a T_m of 56 °C, and a T_c of 26 °C (Table 3).[29]

Table 3. Crystallization (T_c) and Melting (T_m) Temperatures, Crystallinity Degree (X_c), Temperature at the Onset of Thermal Degradation (T_{onset}) and Temperature at a Maximum Mass Loss (T_{max}) of KL, PCL, and Lignin-*g*-PCLs

	T_c (°C)	T_m (°C)	X_c (%)	T_{onset} (°C)	T_{max} (°C)
PCL[26,29]	26	56	73.3		373
KL				232	482
KL-PCL	15	50	34.5	232	409
F_{ins}-PCL		44	2.9	204	403
F1-PCL	33	53	45.9	244	409
F2-PCL	29	52	42.7	249	405
F3-PCL	23	49	45.8	258	408

In the present study, the T_m of all copolymers decreases compared with that of neat PCL likely because the amorphous lignin backbone inhibits the crystallization and regular alignment of the PCL polymer.[26] All copolymers except F_{ins}-PCL present semi-crystalline structures with X_c between 30%−45% and similar T_m at around 50 °C (Table 3). Thereinto, X_c of KL-PCL is smaller than those of F1-PCL, F2-PCL, and F3-PCL but larger than that of F_{ins}-PCL (Table 3), suggesting that fractionating KL to narrower-$Đ_M$ fractions is beneficial to the formation of crystallinities. Combined with the results from Figure 3B,C, as we hypothesized, the lignin MW heterogeneity appears to influence the copolymer structures. However, X_c of lignin-*g*-PCLs from the three representative lignin fractions, F1, F2, and F3, are similar, implying that lignin M_w causes an insignificant effect on copolymer X_c. With respect to the nonrepresentative lignin fraction-derived F_{ins}-PCL, the lowest T_m of 44 °C and extremely low X_c of only 2.9% (inserted image in Figure 5A and Table 3) result from its existence of amorphous hemicellulose, low M_w, and short PCL size. In conclusion, we contend that F_{ins}-PCL is a three-dimensional amorphous network formed by hydrogen bonds between lignin and PCL, while F1-PCL, F2-PCL, and F3-PCL are semi-crystalline copolymers composed of both crystalline and amorphous structures.[27]

Lignin has been frequently used to improve the thermal stability of polymers through copolymerization, such as polyurethanes, poly(arylene ether sulfone), and poly(*n*-butyl acrylate-*co*-methyl methacrylate), *via* multiple mechanisms, including introducing aromatic structures, increasing the copolymer M_w, and the formation of chain-extended polymers at elevated temperatures.[6,53−55] In this study, the thermal stability of lignin-*g*-PCLs were also improved compared with neat PCL (T_{max}: ~400 °C *vs* 373 °C, Figure 5D and Table 3), which is accordant with the result from a previous report.[22] This improved stability is likely attributed to the fact that (*i*) the integration of the lignin moiety enhances the thermal stability of lignin-*g*-PCLs by introducing thermally stable aromatic rings and C−C bonds between lignin subunits that decompose at ~400 °C.[56] It can also be supported by the result that the T_{max} of KL (482 °C) is much higher than that of both copolymers (~400 °C) and neat PCL (373 °C) (Table 3); (*ii*) the conversion of lignin OH groups to ester groups by grafting PCL arms on the lignin backbone has an additional stabilizing effect on the thermal stability of copolymers.[26,52]

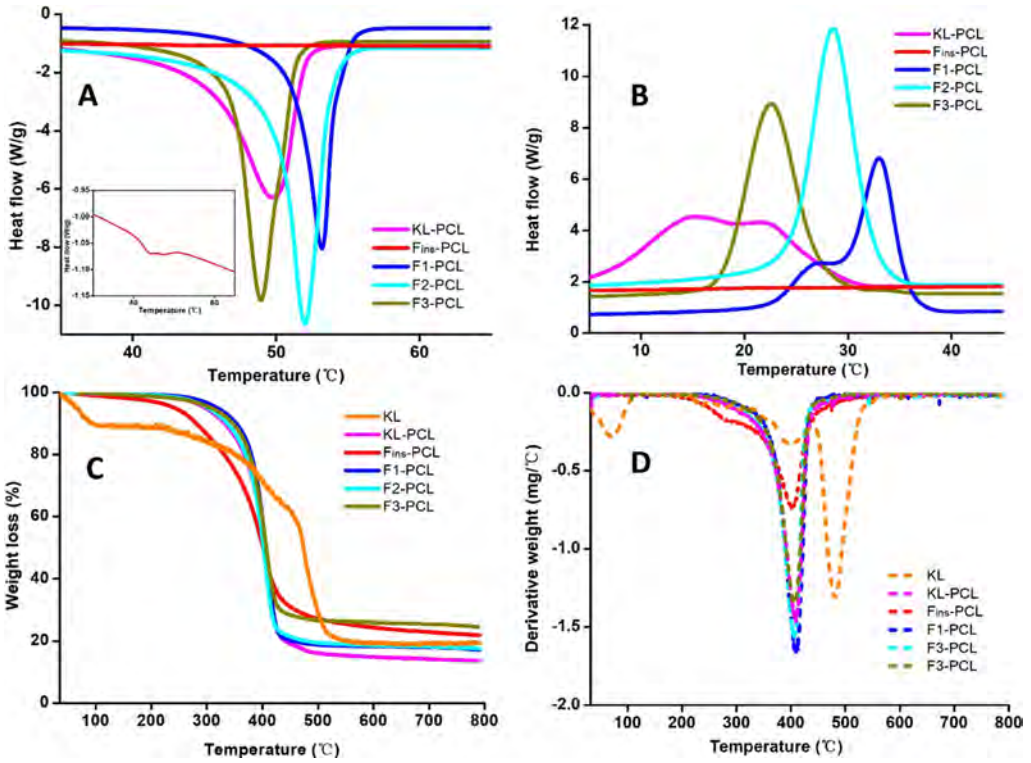

Figure 5. DSC heating (A), DSC cooling (B), TGA (C), and DTG (D) curves of KL and lignin-*g*-PCLs. The inserted figure is the heating curve of F_{ins}-PCL tested by DSC.

https://doi.org/10.1021/acssuschemeng.2c05495
ACS Sustainable Chem. Eng. 2022, 10, 16882−16895

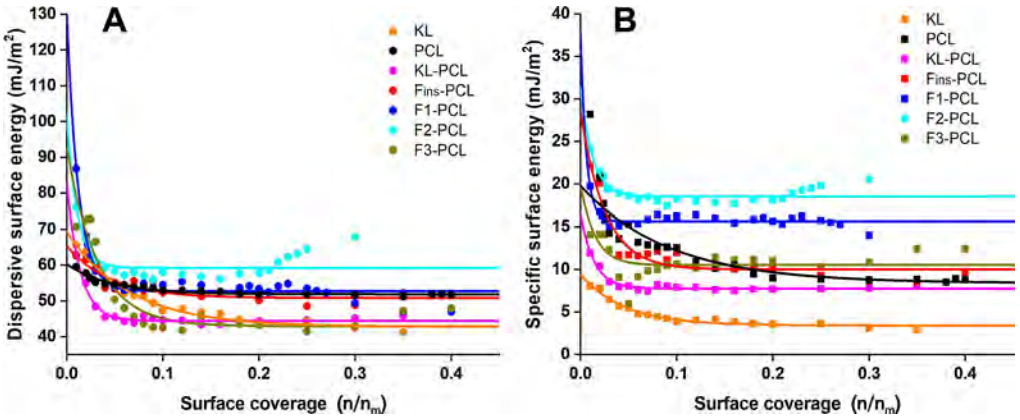

Figure 6. Dispersive (A) and specific (B) surface energy of KL, PCL, and lignin-*g*-PCLs.

Table 4. Minimum, Median (50% percentile of surface energy), and Maximum Values of γ_d and γ_{sp}, Hydrophilicity Index ($\gamma_{sp}/(\gamma_{sp} + \gamma_d)$) and Specific Surface Area of KL and Lignin-*g*-PCLs

	γ_d (mJ/m^2)			γ_{sp} (mJ/m^2)				
samples	Min.	Med.	Max.	Min.	Med.	Max.	$\gamma_{sp}/(\gamma_{sp} + \gamma_d)$	specific surface area (m^2/g)
PCL	53.65	57.64	59.28	8.38	18.31	22.39	0.27	1.10
KL	42.80	47.68	68.91	3.41	4.51	9.29	0.09	6.07
KL-PCL	44.56	51.36	80.85	7.78	9.32	16.00	0.16	1.15
F_{ins}-PCL	50.63	53.24	64.61	10.00	13.34	27.85	0.22	0.85
F1-PCL	52.75	66.28	125.02	2.69	7.01	17.51	0.08	3.42
F2-PCL	59.20	66.54	98.32	18.50	20.74	30.48	0.24	4.77
F3-PCL	42.93	51.96	91.26	10.52	12.18	19.40	0.19	2.85

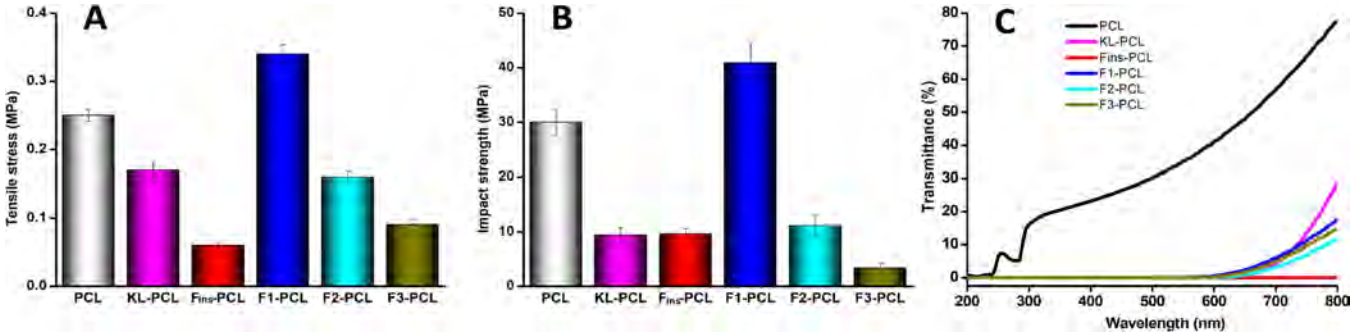

Figure 7. Tensile strength (A), impact strength (B), and UV−vis spectra (C) of PCL and lignin-*g*-PCL films.

Additionally, lignin-*g*-PCLs synthesized by the three representative lignin fractions displaying similar weight loss behaviors with T_{max} at ∼400 °C (Figure 5D and Table 3) indicates that lignin M_w has a negligible influence on the thermal stability of copolymers.

The surface properties of lignin copolymers, such as surface energy (wettability), surface charge, and stability, are critical factors determining the applications of the developed materials. We have evaluated the surface energy and heterogeneity distributions of lignin-*g*-PCLs using iGC. Both the dispersive energy (γ_d) and specific (acid−base) energy (γ_{sp}) of the original KL and the copolymers are exponentially decreased under the lower surface coverage and then tend to be constant under the higher surface coverage (broad range of γ_d and γ_{sp}) in KL and copolymers (Figure 6A,B), indicating highly energetical heterogeneities on their surface.[57] Meanwhile, the median values of γ_d are apparently higher than those of γ_{sp} in all samples (Table 4), implying that PCL, KL, and copolymers are dominated by the *van der Waals* force than dipole−dipole polar force.[58] Compared with PCL and KL, KL-PCL exhibits broader γ_d distributions (Table 4), suggesting that after copolymerization, the surface energetical heterogeneity of lignin-*g*-PCL is intensified. KL-PCL has a greater value of γ_d than KL but smaller than PCL (Table 4), meaning that the PCL segment may be the reason for its intensified dispersive interactions. Among lignin-*g*-PCLs, both F1-PCL and F2-PCL have a relatively higher γ_d (median value: 66.28 and 66.54 mJ/m^2) and larger specific surface area (3.42 and 4.77 m^2/g) than F3-PCL (median value: 51.96 mJ/m^2 and 2.85 m^2/g, Table 4), suggesting that F1-PCL and F2-PCL presumably possess better dispersibility if blended with other nonpolar polymers. The higher median values of γ_d of F1-PCL and F2-PCL than that of F3-PCL could be explained by their larger M_w or lower X_c with more amorphous regions that expose more active groups and intermolecular spaces on the surface. Furthermore, the lowest median value of γ_{sp} of F1-PCL among all lignin-*g*-PCLs (Table 4) means the strongest polar−polar affinity.[59] Additionally, a higher hydrophilicity index, defined as the ratio of $\gamma_{sp}/(\gamma_{sp}$ +

https://doi.org/10.1021/acssuschemeng.2c05495
ACS Sustainable Chem. Eng. 2022, 10, 16882−16895

γ_d), of KL-PCL than that of KL but lower than that of PCL (Table 4) indicates that lignin incorporation can intensify the hydrophobicity of PCL, which might be because lignin introduced aromatic groups to long-chain PCL esters.[59,60] The lowest hydrophilicity index of F1-PCL (Table 4) may be ascribed to the highest content of hydrophobic groups like ester and alkyl groups because of the longest PCL chains. However, although F2-PCL has a longer PCL chain length (more ester and alkyl groups) than F3-PCL, it still exhibits a higher hydrophilicity index (0.24 *vs* 0.19). The reason might be that F3-PCL with a higher X_c is more difficult to be accessed by water molecules.[61] In general, the surface energy of copolymers is affected not only by their M_w but also by the X_c.

The maximum mechanical properties of lignin-*g*-PCL films are 0.34 MPa for tensile strength and 40.92 MPa for impact strength (Table S1), which are lower than those reported in previous studies where the maximum tensile strengths of 1.22[22] and 2.03 MPa.[27] This is likely due to the discrepancies in synthetic conditions, as well as structural features of synthesized copolymers. Compared with the neat PCL films, the F1-PCL film exclusively exhibits higher tensile strength and impact strength (Figure 7A,B). It is likely attributed to the high M_w where a greater number of stable covalent bonds formed and high X_c.[62] However, overall, the result of mechanical properties reveals that incorporation of lignin usually compromises the mechanical properties of lignin-based biocomposites, which is accordant with previous reports.[21,27]

KL is an excellent UV barrier due to the formation of unsaturated ethylene groups and condensed structures, while the intermolecular β−O−4 linkages were cleaved during the pulping process.[63] This UV-blocking function can be imparted to KL-based composites.[64,65] In the current study, all the prepared lignin-*g*-PCL films, including both the nonfractionated and fractionated lignin precursors used, can effectively shield broad-spectrum UV radiation including UV-A (wavelength at 400−320 nm), UV-B (wavelength at 320−280 nm), and UV-C (wavelength at 280−200 nm) regions; on the contrary, the half-transparent neat PCL film shows inferior UV-shielding performance (Figure 7C). Hence, lignin incorporation plays an important role in enhancing the UV-blocking effect of fabricated lignin-*g*-PCL films.

Biodegradability of Lignin-*g*-PCLs. PCL is usually documented as a biodegradable polyester, but the complete degradation could take over 200 days in a landfill and over 120 days in a digester sludge.[66] We evaluated the degradability of lignin-*g*-PCL using an enzymatic hydrolysis approach that is widely employed for PCL and PCL-based polymers.[41,67,68] We have found that lipase can completely hydrolyze the neat PCL within 12 days, which is similar to a previous report of 15 days.[41] However, the degradation of lignin-*g*-PCLs using lipase exhibits much slower degradation rates (Figure 8). The reason might be that the presence of lignin caused a negative influence on the accessibility of lipase to copolymers,[69,70] resulting in a reduced enzyme hydrolysis efficiency. In addition, lipase hydrolysis is affected by polymer structures, for example, M_w, X_c, and chemical composition.[41,71] This has been revealed by the different hydrolysis rates of the copolymers derived from the three representative F1, F2, and F3 fractions, showing that F3-PCL, F2-PCL, and F1-PCL are in the degradation order from high to low. It is likely associated with the differing X_c of PCL segments and M_w of the copolymer. As displayed, the degradation rate of all copolymers is fast in the early stage but slows down in the late stage. This means amorphous regions of copolymers are degraded first because of loose structures, while crystalline regions are degraded later because of the compact alignment and difficult enzymatic accessibility.[71] Furthermore, F_{ins}-PCL presents the lowest degradation rate, which may be attributed to its relatively higher lignin content that is ineffective to lipase hydrolysis and restricts lipase accessibility.

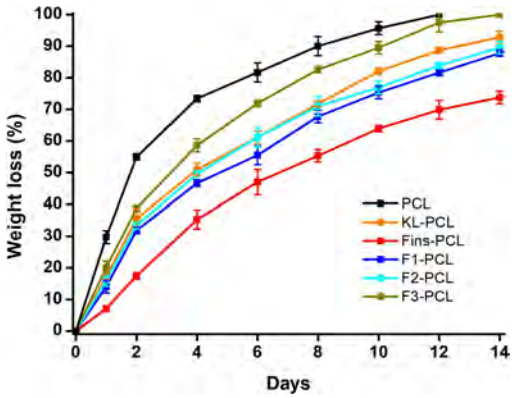

Figure 8. Lipase hydrolysis of neat PCL and lignin-*g*-PCL films.

Application of CFP with Lignin-*g*-PCL for Water/Oil Separation. With the rich OH groups serving as grafting sites, lignin can be chemically modified to substantially reduce hydrophilicity, making it a good candidate for constructing bio-based hydrophobic materials.[72] Lignin has been widely investigated to prepare filtration and adsorption materials for water/oil separation, such as lignin contained wood aerogel/polydimethylsiloxane membrane for chloroform separation from water[73] and silicone-modified lignin particles used as a filler in the filtration apparatus.[74] Lignin-*g*-PCL, as an environmentally friendly biomaterial, has shown potential as surface coatings because of excellent UV-barrier capacity, good dispersibility, favorable film-forming ability, and stable surface characteristics including adhesion strength, abrasion, and gloss.[21,26,48] However, new applications of lignin-*g*-PCL as surface coatings remain to be explored. Combined with the enhanced hydrophobicity determined from iGC, lignin-*g*-PCL was coated on FP to evaluate the ability of purifying oil-polluted water in the current work.

We have found that the WCA of the neat PCL film is lower than that of lignin-*g*-PCL films (Figure S5A), confirming that lignin integration can enhance the hydrophobicity of PCL. This result agrees with the increased dispersive energy of the copolymer measured using iGC previously. We also added SiO_2 and silicone oil to the FP-coating process to further increase the hydrophobicity of CFP. FTIR spectra of the coated FP verify the presence of lignin-*g*-PCLs, SiO_2, and silicone oil on the CFP-C surface (Figure S3). The coated FP by the copolymer, CFP-C, has shown different surface morphologies in comparison to the uncoated FP (Figure 9A,B) in that on the FP surface, cellulose fibers are entangled with each other to form a porous matrix (Figure 9A and S4), while the CFP-C surface is much more compact and smoother due to the filled coating contents such as copolymers, SiO_2, and silicone oil in this case (Figures 9B and S4). The spherical particles on the CFP-C surface might be the SiO_2 particles (Figure 9B). CFP-C becomes more hydrophobic as revealed by the increased WCA with the increase of concentrations of lignin-*g*-PCL/acetone solutions, for example, the WCA reaches up to 120° at a concentration of 1 mg/mL (Figure S5B).

https://doi.org/10.1021/acssuschemeng.2c05495
ACS Sustainable Chem. Eng. 2022, 10, 16882−16895

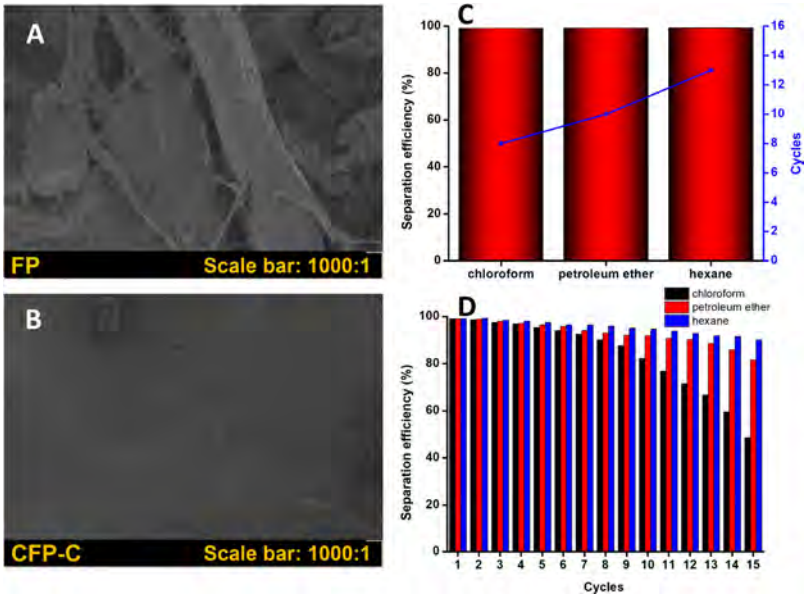

Figure 9. SEM images of FP (A) and CFP-C (B) under a scale bar of 1000; separation efficiencies at the first cycle, cycles with separation efficiencies over 92% (C) and separation efficiencies of CFP-C under 15 cycles (D) for separating chloroform−, petroleum ether−, and hexane−water mixtures.

Moreover, water is adsorbed immediately once contacted with the hydrophilic FP without forming a water drop; a similar phenomenon is observed in CFP-B (Video S1). After FP is coated with PCL and F1-PCL, the surface becomes hydrophobic since WCA over 90° is formed when the water drop contacts the substrate at the very beginning. However, CFP-P displays a much worse water-resistance ability than CFP-C owing to the fact that the water droplet gradually permeates the CFP-P substrate within 1 min, while it holds still on the CFP-C substrate for more than 20 min (Video S1). Hence, we speculate that the lignin portion endows CFP-C with a water barrier, and the hydrophobicity synergistically derives from multiple substances on the surface, including lignin-*g*-PCL, SiO_2, and silicone oil.

For water/oil separation application, CFP with F1-PCL (CFP-C) exhibits the highest water/oil separation efficiency even though the superior performance to other copolymer CFPs is not substantial; besides, CFP with F1-PCL exhibited relatively a higher separation efficiency than CFP with KL-PCL—copolymer without fractionation (Figure S6). The result is likely associated with F1-PCL featuring a higher M_w of lignin (i.e., 4,461 Da) and a longer grafted PCL length (i.e., 40), showing better water/oil separation ability. However, this relationship does not apply to CFPs with F2-PCL (M_w of 3,086 Da and PCL size of 25) and F3-PCL (M_w of 1,691 Da and PCL size of 20) because the structural differences of copolymers and lignin only caused slight influence on the separation efficiency. As a result, taking advantage of the relatively higher hydrophobicity (Figure S5) and water/oil separation efficiency (Figure S6) among all copolymers, CFP-C coated by F1-PCL was chosen to conduct the further water/oil separation experiment. FP (noncoated filter paper) and CFP-P (coated by 1.0 mg/mL PCL/acetone solution) were used as referrals. In the first cycle, CFP-C is able to filter low-surface energy chloroform down to the vial and retain high-surface energy water in the conical funnel, displaying an outstanding separation efficiency of 99.0%; CFP-P otherwise displays a poor separation efficiency of 12.8%; FP filtered most of water because of its hydrophilicity (Figure 9C and Video S2). Thus, CFP-C in this work realized the successful separation of the water/oil mixture *via* a simple and fast conical funnel filtration method. Apart from chloroform, CFP-C also exhibits maximum separation efficiencies of 99.1 and 99.2% for petroleum ether and hexane, respectively, in the first cycle (Figure 9C), showing a universality of CFP-C in water/oil separation. The separation efficiencies are comparable with reported lignin-based two-dimensional filtration biomaterials, such as CFP and membrane.[33,36] For instance, an aerogel membrane fabricated by lignin, trimethoxymethylsilane, graphene oxide, and sodium alginate displayed a maximum separating efficiency above 95% for chloroform, and the separating efficiency was still above 90% after 10 reuses.[36] Moreover, CFP constructed with acetonitrile-extracted lignin and silica particles exhibited a maximum separating efficiency of 98.6% for chloroform (remained 96.6% at the fifth cycle) and above 95% for petroleum ether and hexane.[33] During separation, the lignin component seems to play a water-blocking barrier that stops water on the top, and the modified hydrophobic surface enables the infiltration of the organic solvent through CFP-C. Reusability is a significant parameter for filtration materials applied for wastewater processing. Herein, CFP-C maintains separation efficiencies of above 90% for 8 cycles to chloroform, 12 times to petroleum ether, and 15 times to hexane (Figure 9C). The separation efficiency decreases as cycles progress because coated copolymers and silicon compounds gradually leach out with the organic solvents during each separation process. For petroleum ether−water and hexane−water mixtures, the separation efficiency declines less conspicuously than that for chloroform, still reaching 90.1% at the 15th cycle when separating hexane (Figure 9D). The poorest reusability of CFP-C for chloroform/water separation is attributed by the dissolution of copolymers in chloroform that carries off chemicals from the FP substrate little by little, leading to a reduction of water resistance and hydrophobicity of CFP-C as the cycles increased. Nevertheless, lignin-*g*-PCL is limitedly soluble in

https://doi.org/10.1021/acssuschemeng.2c05495
ACS Sustainable Chem. Eng. 2022, 10, 16882−16895

petroleum ether and hexane, so the reusability of CFP-C is superior. Overall, CFP-C exhibits excellent feasibility and reusability for water/oil separation.

The lignin-*g*-PCL is attractive due to its biodegradability for both lignin and PCL components, low cost, and sustainability. However, the reusability of the CFP with lignin-*g*-PCL for water/oil separation seems variable depending on the solvent used. For example, the separation of chloroform from water is restricted due to the solubility of copolymers in chloroform. The results imply that water/oil separation coating with covalently modified and highly biodegradable copolymers can be achieved with judicious design of the molecular structures.

CONCLUSIONS

KL was fractionated into four lignin fractions with decreasing M_w by the acetone−methanol cosolvent (7:3, *v*/*v*) and hexane, which are F_{ins} (11,188 Da), F1 (4,461 Da), F2 (3,086 Da), and F3 (1,691 Da). Thereof, F_{ins} is a nonrepresentative fraction that contains carbohydrate impurities, while F1, F2, and F3 are representative fractions whose M_w positively correlates with the aliphatic OH content but negatively correlates with the phenolic OH content. Lignin-*g*-PCL copolymers are successfully synthesized with lignin fractions and ε-CL monomers, during which ε-CL is inclined to interact with aliphatic OH in lignin. A higher M_w and a richer aliphatic OH content of lignin are beneficial to the extension of PCL arms and M_w of lignin-*g*-PCLs. Fractionating KL into more homogeneous fractions is conducive to the crystallization of the PCL segment. Generally, M_w and X_c play synergetic roles in thermal, surface, and mechanical properties of lignin-*g*-PCLs, where lignin incorporation improves the thermal stability, hydrophobicity, and UV-blocking ability but slows down the lipase hydrolysis of PCL. Lignin-*g*-PCL, for the first time, was successfully used to separate chloroform−, petroleum ether−, and hexane−water mixtures when coated on a filter paper with a separation efficiency up to 99.2%. Cycles maintaining separation efficiencies above 90% reach up to 15. The structural differences of copolymers derived from fractionated lignins cause minimal influence on the separating efficiency. This study sheds light on the structural influence of lignin on the copolymerization and properties of lignin-*g*-PCL. It also provides important information for the development of lignin-derived composites and lignin valorization.

ASSOCIATED CONTENT

Supporting Information

The Supporting Information is available free of charge at https://pubs.acs.org/doi/10.1021/acssuschemeng.2c05495.

Young's modulus, tensile strength, and impact strength of neat PCL and lignin-*g*-PCL films; fractionation procedure of KL; ^{1}H NMR spectra of lignin-*g*-PCLs; FTIR spectra of FP, CFP-P, and CFP-C; SEM images of FP and CFP-C under scale bars of 105 and 300; WCA of neat PCL, lignin-*g*-PCL films, and CFP-C; and separation efficiencies of CFP with KL-PCL, F_{ins}-PCL, F1-PCL, F2-PCL, and F3-PCL (PDF)

WCA test for FP (MP4)

WCA test for CFP (MP4)

WCA test for CFP-B (MP4)

WCA test for CFP-C (MP4)

Water/chloroform separation experiments with FP, CFP-P, and CFP-C (MP4)

AUTHOR INFORMATION

Corresponding Author

Mi Li − *Center for Renewable Carbon, Department of Forestry, Wildlife and Fisheries, The University of Tennessee, Knoxville, Tennessee 37996, United States;* orcid.org/0000-0001-7523-1266; Email: mli47@utk.edu

Authors

Di Xie − *Center for Renewable Carbon, Department of Forestry, Wildlife and Fisheries, The University of Tennessee, Knoxville, Tennessee 37996, United States*

Yunqiao Pu − *Bioscience Division, Joint Institute of Biological Sciences, Oak Ridge National Laboratory, Oak Ridge, Tennessee 37831, United States*

Xianzhi Meng − *Department of Chemical and Biomolecular Engineering, The University of Tennessee, Knoxville, Tennessee 37996, United States;* orcid.org/0000-0003-4303-3403

Nathan D. Bryant − *Bioscience Division, Joint Institute of Biological Sciences, Oak Ridge National Laboratory, Oak Ridge, Tennessee 37831, United States; Department of Chemical and Biomolecular Engineering, The University of Tennessee, Knoxville, Tennessee 37996, United States*

Kailong Zhang − *Center for Renewable Carbon, Department of Forestry, Wildlife and Fisheries, The University of Tennessee, Knoxville, Tennessee 37996, United States*

Wei Wang − *Department of Mechanical, Aerospace and Biomedical Engineering, The University of Tennessee, Knoxville, Tennessee 37996, United States;* orcid.org/0000-0002-1260-2098

Arthur J. Ragauskas − *Center for Renewable Carbon, Department of Forestry, Wildlife and Fisheries and Department of Chemical and Biomolecular Engineering, The University of Tennessee, Knoxville, Tennessee 37996, United States; Bioscience Division, Joint Institute of Biological Sciences, Oak Ridge National Laboratory, Oak Ridge, Tennessee 37831, United States;* orcid.org/0000-0002-3536-554X

Complete contact information is available at: https://pubs.acs.org/10.1021/acssuschemeng.2c05495

Author Contributions

D.X.: conceptualization, methodology, investigation, formal analysis, data curation, writing-original draft. Y.P.: resources, data curation, writing-review and editing. XM: investigation, writing-review and editing. N.B.: investigation, writing-review and editing. K.Z.: investigation, writing-review and editing. W.W.: resources, writing-review and editing. A.R.: resources, writing-review and editing. M.L.: conceptualization, methodology, supervision, validation, writing-original draft, project administration, and funding acquisition.

Notes

The authors declare no competing financial interest.

ACKNOWLEDGMENTS

We acknowledge the support from the USDA National Institute of Food and Agriculture, Hatch project 7001629, the South-eastern Regional Sun Grant Centre at the University of Tennessee, and the University of Tennessee Agricultural Experiment Station and AgResearch. Oak Ridge National Laboratory is managed by UT-Battelle, LLC under Contract DE-AC05-00OR22725 with the U.S. Department of Energy

REFERENCES

(1) Wise, L. E.; Brown, H. P. *Wood chemistry*; Reinhold Publishing Corporation: New York, 1944.
(2) Constant, S.; Wienk, H. L. J.; Frissen, A. E.; Peinder, P. D.; Boelens, R.; Van Es, D. S.; Grisel, R. J. H.; Weckhuysen, B. M.; Huijgen, W. J. J.; Gosselink, R. J. A.; Bruijnincx, P. C. A. New insights into the structure and composition of technical lignins: A comparative characterisation study. *Green Chem.* **2016**, *18*, 2651−2665.
(3) Rencoret, J.; Prinsen, P.; Gutiérrez, A.; Martínez, A. N. T.; del Río, J. C. Isolation and structural characterization of the milled wood lignin, dioxane lignin, and cellulolytic lignin preparations from brewer's spent grain. *J. Agric. Food Chem.* **2015**, *63*, 603−613.
(4) Brebu, M.; Tamminen, T.; Spiridon, I. Thermal degradation of various lignins by TG-MS/FTIR and Py-GC-MS. *J. Anal. Appl. Pyrolysis* **2013**, *104*, 531−539.
(5) Gellerstedt, G. Softwood kraft lignin: Raw material for the future. *Ind. Crops Prod.* **2015**, *77*, 845−854.
(6) Sen, S.; Patil, S.; Argyropoulos, D. S. Thermal properties of lignin in copolymers, blends, and composites: a review. *Green Chem.* **2015**, *17*, 4862−4887.
(7) Naseem, A.; Tabasum, S.; Zia, K. M.; Zuber, M.; Ali, M.; Noreen, A. Lignin-derivatives based polymers, blends and composites: A review. *Int. J. Biol. Macromol.* **2016**, *93*, 296−313.
(8) Kong, F.; Wang, S.; Price, J. T.; Konduri, M. K. R.; Fatehi, P. Water soluble kraft lignin-acrylic acid copolymer: synthesis and characterization. *Green Chem.* **2015**, *17*, 4355−4366.
(9) Martín-Sampedro, R.; Santos, J. I.; Fillat, Ú.; Wicklein, B.; Eugenio, M. E.; Ibarra, D. Characterization of lignins from Populus alba L. generated as by-products in different transformation processes: Kraft pulping, organosolv and acid hydrolysis. *Int. J. Biol. Macromol.* **2019**, *126*, 18−29.
(10) Zhang, R.; Du, Q.; Wang, L.; Zheng, Z.; Guo, L.; Zhang, X.; Yang, X.; Yu, H. Unlocking the response of lignin structure for improved carbon fiber production and mechanical strength. *Green Chem.* **2019**, *21*, 4981−4987.
(11) Gigli, M.; Crestini, C. Fractionation of industrial lignins: opportunities and challenges. *Green Chem.* **2020**, *22*, 4722−4746.
(12) Jiang, X.; Abbati de Assis, C.; Kollman, M.; Sun, R.; Jameel, H.; Chang, H.-M.; Gonzalez, R. Lignin fractionation from laboratory to commercialization: chemistry, scalability and techno-economic analysis. *Green Chem.* **2020**, *22*, 7448−7459.
(13) Tindall, G. W.; Chong, J.; Miyasato, E.; Thies, M. C. Fractionating and purifying softwood kraft lignin with aqueous renewable solvents: liquid−liquid equilibrium for the lignin-ethanol-water system. *ChemSusChem* **2020**, *13*, 4587−4594.
(14) Wang, Y.-Y.; Li, M.; Wyman, C. E.; Cai, C. M.; Ragauskas, A. J. Fast fractionation of technical lignins by organic cosolvents. *ACS Sustainable Chem. Eng.* **2018**, *6*, 6064−6072.
(15) Izaguirre, N.; Gordobil, O.; Robles, E.; Labidi, J. Enhancement of UV absorbance and mechanical properties of chitosan films by the incorporation of solvolytically fractionated lignins. *Int. J. Biol. Macromol.* **2020**, *155*, 447−455.
(16) Wang, G.; Pang, T.; Xia, Y.; Liu, X.; Li, S.; Parvez, A. M.; Kong, F.; Si, C. Subdivision of bamboo kraft lignin by one-step ethanol fractionation to enhance its water-solubility and antibacterial performance. *Int. J. Biol. Macromol.* **2019**, *133*, 156−164.
(17) Delgado, N.; Ysambertt, F.; Ochoa, R.; Chavez, G.; Bravo, B.; Santos, J.; Garcia, D. E. Esterified lignins from Pinus caribaea as bentonite-dispersing agents. *Clay Miner.* **2018**, *53*, 41−51.
(18) Ikeo, Y.; Aoki, K.; Kishi, H.; Matsuda, S.; Murakami, A. Nano clay reinforced biodegradable plastics of PCL starch blends. *Polym. Adv. Technol.* **2006**, *17*, 940−944.
(19) Labet, M.; Thielemans, W. Synthesis of polycaprolactone: a review. *Chem. Soc. Rev.* **2009**, *38*, 3484−3504.
(20) Li, P.; Fu, L.; Liao, Z.; Peng, Y.; Ning, C.; Gao, C.; Zhang, D.; Sui, X.; Lin, Y.; Liu, S.; Hao, C.; Guo, Q. Chitosan hydrogel/3D-printed poly(ε-caprolactone) hybrid scaffold containing synovial mesenchymal stem cells for cartilage regeneration based on tetrahedral framework nucleic acid recruitment. *Biomaterials* **2021**, *278*, 121131−121131.
(21) Jang, S.-H.; Kim, D.-H.; Park, D. H.; Kim, O. Y.; Hwang, S.-H. Construction of sustainable polyurethane-based gel-coats containing poly(ε-caprolactone)-grafted lignin and their coating performance. *Prog. Org. Coat.* **2018**, *120*, 234−239.
(22) Tian, J.; Yang, Y.; Song, J. Grafting polycaprolactone onto alkaline lignin for improved compatibility and processability. *Int. J. Biol. Macromol.* **2019**, *141*, 919−926.
(23) Liang, R.; Zhao, J.; Li, B.; Cai, P.; Loh, X. J.; Xu, C.; Chen, P.; Kai, D.; Zheng, L. Implantable and degradable antioxidant poly(ε-caprolactone)-lignin nanofiber membrane for effective osteoarthritis treatment. *Biomaterials* **2020**, *230*, No. 119601.
(24) Wang, D.; Jang, J.; Kim, K.; Kim, J.; Park, C. B. "Tree to Bone:" Lignin/Polycaprolactone Nanofibers for Hydroxyapatite Biomineralization. *Biomacromolecules* **2019**, *20*, 2684−2693.
(25) Li, M.; Pu, Y.; Chen, F.; Ragauskas, A. J. Synthesis and Characterization of Lignin-grafted-poly(ε-caprolactone) from Different Biomass Sources. *New Biotechnol.* **2021**, *60*, 189−199.
(26) Liu, X.; Zong, E.; Jiang, J.; Fu, S.; Wang, J.; Xu, B.; Li, W.; Lin, X.; Xu, Y.; Wang, C.; Chu, F. Preparation and characterization of Lignin-graft-poly (ε-caprolactone) copolymers based on lignocellulosic butanol residue. *Int. J. Biol. Macromol.* **2015**, *81*, 521−529.
(27) Laurichesse, S.; Avérous, L. Synthesis, thermal properties, rheological and mechanical behaviors of lignins-grafted-poly(ε-caprolactone). *Polymer* **2013**, *54*, 3882−3890.
(28) Pérez-Camargo, R. A.; Saenz, G.; Laurichesse, S.; Casas, M. T.; Puiggalí, J.; Avérous, L.; Müller, A. J. Nucleation, crystallization, and thermal fractionation of poly(ε-caprolactone)-grafted-lignin: effects of grafted chains length and lignin content. *J. Polym. Sci., Part B: Polym. Phys.* **2015**, *53*, 1736−1750.
(29) Abdollahi, M.; Bairami Habashi, R.; Mohsenpour, M. Poly(ε-caprolactone) chains grafted from lignin, hydroxymethylated lignin and silica/lignin hybrid macroinitiators: Synthesis and characterization of lignin-based thermoplastic copolymers. *Ind. Crops Prod.* **2019**, *130*, 547−557.
(30) Duval, A.; Layrac, G.; Zomeren, A.; Smit, A. T.; Pollet, E.; Avérous, L. Isolation of low dispersity fractions of acetone organosolv lignins to understand their reactivity: towards aromatic building blocks for polymers synthesis. *ChemSusChem* **2021**, *14*, 387−397.
(31) Liu, Z.-H.; Hao, N.; Shinde, S.; Pu, Y.; Kang, X.; Ragauskas, A. J.; Yuan, J. S. Defining lignin nanoparticle properties through tailored lignin reactivity by sequential organosolv fragmentation approach (SOFA). *Green Chem.* **2019**, *21*, 245−260.
(32) Pang, T.; Wang, G.; Sun, H.; Sui, W.; Si, C. Lignin fractionation: Effective strategy to reduce molecule weight dependent heterogeneity for upgraded lignin valorization. *Ind. Crops Prod.* **2021**, *165*, No. 113442.
(33) Gong, X.; Meng, Y.; Zhu, J.; Wang, X.; Lu, J.; Cheng, Y.; Tao, Y.; Wang, H. Construct a stable super-hydrophobic surface through acetonitrile extracted lignin and nano-silica and its application in oil-water separation. *Ind. Crops Prod.* **2021**, *166*, No. 113471.
(34) Yue, Y.; Wang, Y.; Li, J.; Cheng, W.; Han, G.; Lu, T.; Huang, C.; Wu, Q.; Jiang, J. High strength and ultralight lignin-mediated fire-resistant aerogel for repeated oil/water separation. *Carbon* **2022**, *193*, 285−297.

https://doi.org/10.1021/acssuschemeng.2c05495
ACS Sustainable Chem. Eng. 2022, 10, 16882−16895

(35) Cao, M.; Hu, Y.; Cheng, W.; Huan, S.; Bai, T.; Niu, Z.; Zhao, Y.; Yue, G.; Zhao, Y.; Han, G. Lignin-based multi-scale cellular aerogels assembled from co-electrospun nanofibers for oil/water separation and energy storage. *Chem. Eng. J.* **2022**, No. 135233.
(36) Jiang, Y.-H.; Zhang, Y.-Q.; Gao, C.; An, Q.-D.; Xiao, Z.-Y.; Zhai, S.-R. Superhydrophobic aerogel membrane with integrated functions of biopolymers for efficient oil/water separation. *Sep. Purif. Technol.* **2022**, *282*, No. 120138.
(37) Meng, X.; Crestini, C.; Ben, H.; Hao, N.; Pu, Y.; Ragauskas, A. J.; Argyropoulos, D. S. Determination of hydroxyl groups in biorefinery resources via quantitative ^{31}P NMR spectroscopy. *Nat. Protoc.* **2019**, *14*, 2627−2647.
(38) Standard test method for tensile properties of thin plastic sheeting. West Conshohocken, 2010, (West Conshohocken), PA 19428-2959, United States.
(39) Korbag, I.; Mohamed Saleh, S. Studies on mechanical and biodegradability properties of PVA/lignin blend films. *Int. J. Environ. Stud.* **2016**, *73*, 18−24.
(40) Yang, W.; Qi, G.; Ding, H.; Xu, P.; Dong, W.; Zhu, X.; Zheng, T.; Ma, P. Biodegradable poly (lactic acid)-poly (ε-caprolactone)-nanolignin composite films with excellent flexibility and UV barrier performance. *Compos. Commun.* **2020**, *22*, No. 100497.
(41) Ashton, J. H.; Mertz, J. A. M.; Harper, J. L.; Slepian, M. J.; Mills, J. L.; McGrath, D. V.; Vande Geest, J. P. Polymeric endoaortic paving: Mechanical, thermoforming, and degradation properties of polycaprolactone/polyurethane blends for cardiovascular applications. *Acta Biomater.* **2011**, *7*, 287−294.
(42) Wu, H.; Wu, L.; Lu, S.; Lin, X.; Xiao, H.; Ouyang, X.; Cao, S.; Chen, L.; Huang, L. Robust superhydrophobic and superoleophilic filter paper via atom transfer radical polymerization for oil/water separation. *Carbohydr. Polym.* **2018**, *181*, 419−425.
(43) Schuerch, C. The solvent properties of liquids and their relation to the solubility, swelling, isolation and fractionation of lignin. *J. Am. Chem. Soc.* **1952**, *74*, 5061−5067.
(44) Ebrahimi Majdar, R.; Ghasemian, A.; Resalati, H.; Saraeian, A.; Crestini, C.; Lange, H. Case study in kraft lignin fractionation: "structurally purified" lignin fractionsnthe role of solvent H-bonding affinity. *ACS Sustainable Chem. Eng.* **2020**, *8*, 16803−16813.
(45) Tagami, A.; Gioia, C.; Lauberts, M.; Budnyak, T.; Moriana, R.; Lindström, M. E.; Sevastyanova, O. Solvent fractionation of softwood and hardwood kraft lignins for more efficient uses: Compositional, structural, thermal, antioxidant and adsorption properties. *Ind. Crops Prod.* **2019**, *129*, 123−134.
(46) Rohde, V.; Böringer, S.; Tübke, B.; Adam, C.; Dahmen, N.; Schmiedl, D. Fractionation of three different lignins by thermal separation techniques-A comparative study. *Global Change Biol.* **2019**, *11*, 206−217.
(47) Sadeghifar, H.; Ragauskas, A. Perspective on technical lignin fractionation. *ACS Sustainable Chem. Eng.* **2020**, *8*, 8086−8101.
(48) Najarro, M. C.; Nikolic, M.; Iruthayaraj, J.; Johannsen, I. Tuning the lignin-caprolactone copolymer for coating metal surfaces. *ACS Appl. Polym. Mater.* **2020**, *2*, 5767−5778.
(49) Antonino, L. D.; Gouveia, J. R.; de Sousa Júnior, R. R.; Garcia, G. E. S.; Gobbo, L. C.; Tavares, L. B.; Dos Santos, D. J. Reactivity of aliphatic and phenolic hydroxyl groups in kraft lignin towards 4,4' MDI. *Molecules* **2021**, *26*, 2131.
(50) Kuroda, K.; Kunimura, H.; Fukaya, Y.; Nakamura, N.; Ohno, H. ^{1}H NMR evaluation of polar and nondeuterated ionic liquids for selective extraction of cellulose and xylan from wheat bran. *ACS Sustainable Chem. Eng.* **2014**, *2*, 2204−2210.
(51) Shi, Z.; Xu, G.; Deng, J.; Dong, M.; Murugadoss, V.; Liu, C.; Shao, Q.; Wu, S.; Guo, Z. Structural characterization of lignin from D. sinicus by FTIR and NMR techniques. *Green Chem. Lett. Rev.* **2019**, *12*, 235−243.
(52) Hirose, S.; Hatakeyama, T.; Izuta, Y.; Hatakeyama, H. Hatakeyama, TG-FTIR studies on lignin-based polycaprolactones: Speciality Polymers. *J. Therm. Anal. Calorim.* **2002**, *70*, 853−860.
(53) Argyropoulos, D. S.; Sadeghifar, H.; Cui, C.; Sen, S. Synthesis and characterization of poly(arylene ether sulfone) kraft lignin heat stable copolymers. *ACS Sustainable Chem. Eng.* **2014**, *2*, 264−271.
(54) Liu, X.; Wang, J.; Li, S.; Zhuang, X.; Xu, Y.; Wang, C.; Chu, F. Preparation and properties of UV-absorbent lignin graft copolymer films from lignocellulosic butanol residue. *Ind. Crops Prod.* **2014**, *52*, 633−641.
(55) Evtuguin, D. V.; Andreolety, J. P.; Gandini, A. Polyurethanes based on oxygen-organosolv lignin. *Eur. Polym. J.* **1998**, *34*, 1163−1169.
(56) Mohamad Aini, N. A.; Othman, N.; Hussin, M. H.; Sahakaro, K.; Hayeemasae, N. Effect of extraction methods on the molecular structure and thermal stability of kenaf (Hibiscus cannabinus core) biomass as an alternative bio-filler for rubber composites. *Int. J. Biol. Macromol.* **2020**, *154*, 1255−1264.
(57) Das, S. C.; Stewart, P. J. Characterising surface energy of pharmaceutical powders by inverse gas chromatography at finite dilution. *J. Pharm. Pharmacol.* **2012**, *64*, 1337−1348.
(58) Legras, A.; Kondor, A.; Alcock, M.; Heitzmann, M. T.; Truss, R. W. Inverse gas chromatography for natural fibre characterisation: dispersive and acid-base distribution profiles of the surface energy. *Cellulose* **2017**, *24*, 4691−4700.
(59) Niu, C.; Xia, W.; Peng, Y. Analysis of coal wettability by inverse gas chromatography and its guidance for coal flotation. *Fuel* **2018**, *228*, 290−296.
(60) Gamelas, J. A. F.; Duarte, G. V.; Ferreira, P. J. Inverse gas chromatography and XPS of extracted kraft pulps. *Int. J. Sociol. Lang.* **2012**, *218*, No. 0126.
(61) Michael, I. Accessibility and crystallnity of cellulose. *BioResources* **2009**, *4*, 1168−1177.
(62) Hamada, T.; Hasegawa, S.; Fukasawa, H.; Sawada, S.-I.; Koshikawa, H.; Miyashita, A.; Maekawa, Y. Poly(ether ether ketone) (PEEK)-based graft-type polymer electrolyte membranes having high crystallinity for high conducting and mechanical properties under various humidified conditions. *J. Mater. Chem. A* **2015**, *3*, 20983−20991.
(63) Lin, M.; Yang, L.; Zhang, H.; Xia, Y.; He, Y.; Lan, W.; Ren, J.; Yue, F.; Lu, F. Revealing the structure-activity relationship between lignin and anti-UV radiation. *Ind. Crops Prod.* **2021**, *174*, No. 114212.
(64) Klapiszewski, Ł.; Podkościelna, B.; Goliszek, M.; Kubiak, A.; Młynarczyk, K.; Jesionowski, T. Synthesis, characterization and aging tests of functional rigid polymeric biocomposites with kraft lignin. *Int. J. Biol. Macromol.* **2021**, *178*, 344−353.
(65) Parit, M.; Du, H.; Zhang, X.; Jiang, Z. Flexible, transparent, UV-protecting, water-resistant nanocomposite films based on polyvinyl alcohol and kraft lignin-grafted cellulose nanofibers. *ACS Appl. Polym. Mater.* **2022**, *4*, 3587−3597.
(66) Federle, T. W.; Barlaz, M. A.; Pettigrew, C. A.; Kerr, K. M.; Kemper, J. J.; Nuck, B. A.; Schechtman, L. A. Anaerobic biodegradation of aliphatic polyesters: poly(3-hydroxybutyrate-co-3-hydroxyoctanoate) and poly(ε-caprolactone). *Biomacromolecules* **2002**, *3*, 813−822.
(67) Ben Abdallah, A.; Kallel, A.; Gamaoun, F.; Tcharkhtchi, A. Enzymatic hydrolysis of poly (caprolactone) and its blend with styrene−butadiene−styrene (40% PCL/60% SBS). *J. Polym. Environ.* **2019**, *27*, 2341−2351.
(68) Liu, Q.; Wang, H.; Chen, L.; Li, W.; Zong, Y.; Sun, Y.; Li, Z. Enzymatic degradation of fluorinated poly(ε-caprolactone) (PCL) block copolymer films with improved hydrophobicity. *Polym. Degrad. Stab.* **2019**, *165*, 27−34.
(69) Jia, Y.; Yang, C.; Shen, B.; Ling, Z.; Huang, C.; Li, X.; Lai, C.; Yong, Q. Comparative study on enzymatic digestibility of acid-pretreated poplar and larch based on a comprehensive analysis of the lignin-derived recalcitrance. *Bioresour. Technol.* **2021**, *319*, 124225−124225.
(70) Tian, D.; Guo, Y.; Huang, M.; Zhao, L.; Deng, S.; Deng, O.; Zhou, W.; Hu, J.; Shen, F. Bacterial cellulose/lignin nanoparticles composite films with retarded biodegradability. *Carbohydr. Polym.* **2021**, *274*, 118656−118656.

(71) Yoshida, M.; Liu, Y.; Uchida, S.; Kawarada, K.; Ukagami, Y.; Ichinose, H.; Kaneko, S.; Fukuda, K. Effects of cellulose crystallinity, hemicellulose, and lignin on the enzymatic hydrolysis of Miscanthus sinensis to monosaccharides. *Biosci., Biotechnol., Biochem.* **2008**, *72*, 805−810.
(72) Sun, H.; Liu, Z.; Liu, K.; Gibril, M. E.; Kong, F.; Wang, S. Lignin-based superhydrophobic melamine resin sponges and their application in oil/water separation. *Ind. Crops Prod.* **2021**, *170*, No. 113798.
(73) Wang, K.; Liu, X.; Tan, Y.; Zhang, W.; Zhang, S.; Li, J. Two-dimensional membrane and three-dimensional bulk aerogel materials via top-down wood nanotechnology for multibehavioral and reusable oil/water separation. *Chem. Eng. J.* **2019**, *371*, 769−780.
(74) Yu, M.; Mishra, D.; Cui, Z.; Wang, X.; Lu, Q. Recycling papermill waste lignin into recyclable and flowerlike composites for effective oil/water separation. *Composites, Part B* **2021**, *216*, No. 108884.

https://doi.org/10.1021/acssuschemeng.2c05495
ACS Sustainable Chem. Eng. 2022, 10, 16882−16895